

RKKY interaction in helical higher-order topological insulators

Sha Jin(金莎), Jian Li(李健), Qing-Xu Li(李清旭), and Jia-Ji Zhu(朱家骥)

Citation: Chin. Phys. B, 2024, 33 (**7**): 077503. DOI: 10.1088/1674-1056/ad3ef9
Journal homepage: http://cpb.iphy.ac.cn; http://iopscience.iop.org/cpb

What follows is a list of articles you may be interested in

Magnetic and electronic properties of bulk and two-dimensional $FeBi_2Te_4$: A first-principles study

Qianqian Wang(王倩倩), Jianzhou Zhao(赵建洲), Weikang Wu(吴维康), Yinning Zhou(周胤宁), Qile Li, Mark T. Edmonds, and Shengyuan A. Yang(杨声远)
Chin. Phys. B, 2023, 32 (**8**): 087506. DOI: 10.1088/1674-1056/acd522

Magnetic ordering induced magnetodielectric effect in $Ho_2Cu_2O_5$ and $Yb_2Cu_2O_5$

Hao Jin(金昊), Shuai Huang(黄帅), Kai-Qi Wan(万凯奇), Chang-Ming Zhu(朱长明),Hai-Ou Wang(王海欧), Kun-Peng Su(苏昆朋), and De-Xuan Huo(霍德璇)
Chin. Phys. B, 2023, 32 (**6**): 067504. DOI: 10.1088/1674-1056/ac904a

Strong spin frustration and magnetism in kagomé antiferromagnets $LnCu_3(OH)_6Br_3$ (*Ln*=Nd, Sm, and Eu)

Jin-Qun Zhong(钟金群), Zhen-Wei Yu(余振伟), Xiao-Yu Yue(岳小宇), Yi-Yan Wang(王义炎), Hui Liang(梁慧), Yan Sun(孙燕), Dan-Dan Wu(吴丹丹), Zong-Ling Ding(丁宗玲), Jin Sun(孙进), Xue-Feng Sun(孙学峰), and Qiu-Ju Li(李秋菊)
Chin. Phys. B, 2023, 32 (**4**): 047505. DOI: 10.1088/1674-1056/acb9e8

Slight Co-doping tuned magnetic and electric properties on cubic $BaFeO_3$ single crystal

Shijun Qin(覃湜俊), Bowen Zhou(周博文), Zhehong Liu(刘哲宏), Xubin Ye(叶旭斌), Xueqiang Zhang(张雪强), Zhao Pan(潘昭), and Youwen Long(龙有文)
Chin. Phys. B, 2022, 31 (**9**): 097503. DOI: 10.1088/1674-1056/ac7549

Magnetic and magnetocaloric effect in a stuffed honeycomb polycrystalline antiferromagnet $GdInO_3$

Yao-Dong Wu(吴耀东), Wei-Wei Duan(段薇薇), Qiu-Yue Li(李秋月), Yong-Liang Qin(秦永亮),Zhen-Fa Zi(訾振发), and Jin Tang(汤进)
Chin. Phys. B, 2022, 31 (**6**): 067501. DOI: 10.1088/1674-1056/ac43a1

RKKY interaction in helical higher-order topological insulators

Sha Jin(金莎)[1], Jian Li(李健)[1,2,3], Qing-Xu Li(李清旭)[1,2,3], and Jia-Ji Zhu(朱家骥)[1,2,3,†]

[1] *School of Science, Chongqing University of Posts and Telecommunications, Chongqing* 400065, *China*
[2] *Institute for Advanced Sciences, Chongqing University of Posts and Telecommunications, Chongqing* 400065, *China*
[3] *Southwest Center for Theoretical Physics, Chongqing University, Chongqing* 401331, *China*

(Received 27 February 2024; revised manuscript received 13 April 2024; accepted manuscript online 16 April 2024)

We theoretically investigate the Ruderman–Kittel–Kasuya–Yosida (RKKY) interaction in helical higher-order topological insulators (HOTIs), revealing distinct behaviors mediated by hinge and Dirac-type bulk carriers. Our findings show that hinge-mediated interactions consist of Heisenberg, Ising, and Dzyaloshinskii–Moriya (DM) terms, exhibiting a decay with impurity spacing z and oscillations with Fermi energy $\varepsilon_{\rm F}$. These interactions demonstrate ferromagnetic behaviors for the Heisenberg and Ising terms and alternating behavior for the DM term. In contrast, bulk-mediated interactions include Heisenberg, twisted Ising, and DM terms, with a conventional cubic oscillating decay. This study highlights the nuanced interplay between hinge and bulk RKKY interactions in HOTIs, offering insights into designs of next-generation quantum devices based on HOTIs.

Keywords: magnetic impurity interactions, magnetic ordering, spintronics, topological phases

PACS: 75.30.Hx, 75.10.–b, 85.75.d, 03.65.Vf **DOI:** 10.1088/1674-1056/ad3ef9

1. Introduction

The higher-order topological insulators (HOTIs) describe topological materials of d-dimensional insulated bulk and $(d-n)$-dimensional gapless boundary states.[1,2] There are zero-dimensional gapless corner states in two-dimensional (2D) second-order topological insulators[3–6] and three-dimensional (3D) third-order topological insulators,[7,8] and one-dimensional (1D) gapless hinge states in 3D second-order topological insulators.[9–11] HOTIs can be understood as a special kind of topological crystalline insulators (TCIs). For example, one can turn SnTe, a well-known topological crystalline insulator, into a HOTI by reducing temperature or applying uniaxial strain to gap out the Dirac cones of surfaces.[12] Compared with the TCI, the HOTI possesses higher symmetry beyond the crystalline symmetry. For instance, a pristine TCI, the cubic SnTe, is protected by mirror symmetry.[13,14] In contrast, the related HOTI, the strained octahedral SnTe, is protected by both mirror symmetry and time-reversal symmetry.[12] The topological invariants of the HOTIs can be interpreted physically by the electric multipole moments, which further extends the dipole moment theory in TCIs.[15] Like the ordinary topological insulator (TI) with robust $(d-1)$-dimensional boundary states, the HOTIs possess robust $(d-n)$-dimensional boundary states which can also survive defects, impurities, or other perturbations. For instance, the $Pb_{0.67}Sn_{0.33}Se$ bulk crystal holds 1D nontrivial hinge states with a striking robustness to defects, strong magnetic fields, and elevated temperatures.[16] The robustness to perturbations makes HOTIs promising materials for designing high-stable electronic or spintronic devices.

One can break or preserve the time-reversal symmetry to switch the 1D hinge state in 3D second-order topological insulators between chiral and helical regimes. The chiral hinge states are electrons propagating unidirectionally like the edge states of the 2D quantum Hall effect or the quantum anomalous Hall effect. The helical hinge states are Kramers pairs counter-propagating like the edge states of a 2D quantum spin Hall effect,[17] which are also spin–momentum locked and free from back-scattering. The unique spin–momentum locking and counter-propagating currents of helical hinge states allow the design of a helical nanorod which has exactly n-channels of ballistic transport[18] and the spin manipulation based on spin–momentum locking.[19,20] The helical hinge modes may have different configurations; for example, there are two possible helical hinge mode configurations in Bi,[21] where one configuration has C_2 symmetry and time-reversal symmetry and the other only has the time-reversal symmetry. The various configurations of helical states offer the possibility of designing devices by different helical circuits. The helical hinge states have already been realized in materials such as bismuth,[22] SnTe,[12] α-Bi_4Br_4,[23,24] and $MoTe_2$.[25] The helical modes can also be achieved by methods of artificial manipulation, e.g., using bismuth-halide chains by the van der Waals stacking,[26] an array of weakly tunnel-coupled Rashba nanowires,[27] or a C_6-symmetric topological crystalline metamaterial based on the acoustic samples.[28]

Ruderman–Kittel–Kasuya–Yosida (RKKY) interaction describes the exchange coupling between magnetic impurities mediated by the itinerant carriers in the host material. The RKKY interaction has been extensively investigated in various systems such as low-dimensional quantum

†Corresponding author. E-mail: zhujj@cqupt.edu.cn

© 2024 Chinese Physical Society and IOP Publishing Ltd

structures,[29,30] graphene and Dirac semimetals,[31,32] topological insulators,[33,34] Weyl semimetals,[35,36] and topological crystalline insulators.[37–39] The boundary effects in topological materials are predicted to be highly intriguing. HOTIs possess 1D topological hinge states that may offer a unique RKKY interaction resilient to perturbations. Additionally, varying configurations of helical hinges in HOTIs can serve as a versatile platform for magnetic switching through RKKY interaction.

In this work, we focus on the RKKY interaction between magnetic impurities positioned in the helical hinge of a 3D second-order TI. We carefully analyze the system and describe the RKKY interaction not only mediated by the hinge states but also by the bulk states. By utilizing Green's function technique and the low-energy effective Hamiltonian of a 3D second-order TI,[12] we can arrive at the analytical expressions of the hinge and bulk RKKY interactions. The hinge RKKY interaction consists of three terms: the conventional Heisenberg type interaction, the Dzyaloshinskii–Moriya (DM) type interaction along the certain direction, and the Ising type interaction perpendicular to the hinge. The strength of the hinge RKKY interaction is linearly proportional to the reciprocal of impurity spacing and shows a sinusoidal pattern of the product of Fermi energy and impurity spacing. The hinge RKKY interaction exhibits two distinct branches, with the only difference being the sign of the DM interaction at equal impurity spacing. The opposite sign of the DM term reflects the helical nature of the hinge states. The bulk RKKY interaction consists of the conventional Heisenberg-type, twisted Ising-type and DM-type interactions. The strength of the bulk RKKY interaction decreases with the impurity spacing R^3 and also shows a sinusoidal pattern related to Fermi energy and impurity spacing. The interplay between the hinge and bulk RKKY interaction allows for developing several quantum devices with varying hinge setups.

2. Model

We consider a helical HOTI, which has a square cross-section in xy plane but periodic boundary conditions in z direction as shown in Fig. 1. The bulk and surface states are insulated, while the helical hinge states along the z direction are conductive of the counter-propagating helical Kramers pairs. The magnetic impurities are located at the hinges.

The Hamiltonian of itinerant carriers from the helical hinge state reads[12]

$$\begin{aligned}\mathcal{H}(k_z) = {} & \rho_0\tau_x\sigma_x(-\mathrm{i}\partial_x) + \rho_0\tau_x\sigma_y(-\mathrm{i}\partial_y) + \rho_0\tau_x\sigma_z k_z \\ & + \rho_0\tau_z\sigma_0\delta_1 + \rho_z\tau_y\sigma_0\delta_2, \end{aligned} \tag{1}$$

where σ_0 is the unit matrix, and σ_i $(i = x, y, z)$ are the Pauli matrices acting on spin degree of freedom, τ_i the Pauli matrices acting on the d and f orbits, ρ_0 the unit matrix,

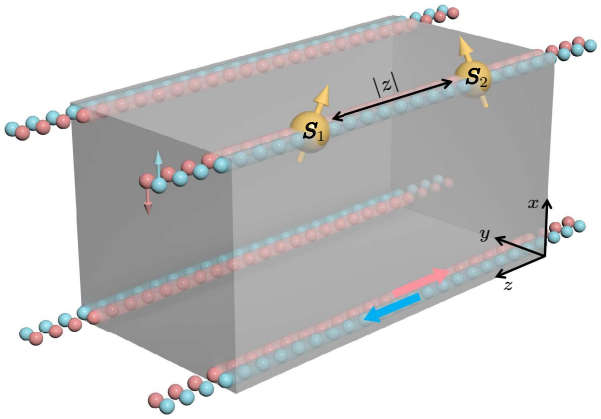


Fig. 1. Diagram of magnetic impurities in the helical hinge of HOTIs. The periodic boundary conditions in the z direction are assumed. The insulated bulk and surface states are painted as gray, while the helical hinge states consisting of Kramers pairs are denoted by colorful balls. The blue (pink) balls stand for carriers with spin up (down). Blue and pink arrows along the z axis mark the direction of motion of up-spin and down-spin carriers. The large yellow balls denote magnetic impurities with magnetic orientation.

and ρ_i the Pauli matrices acting on the $\mathrm{d}_{x^2-y^2}(\mathrm{f}_{(x^2-y^2)z})$ and d_{xy} (f_{xyz}) orbitals, respectively. The basis of the Hamiltonian (1) is $(|\mathrm{d}_{x^2-y^2},\uparrow\rangle,\ |\mathrm{d}_{x^2-y^2},\downarrow\rangle,\ |\mathrm{f}_{(x^2-y^2)z},\uparrow\rangle,\ |\mathrm{f}_{(x^2-y^2)z},\downarrow\rangle,\ |\mathrm{d}_{xy},\uparrow\rangle, |\mathrm{d}_{xy},\downarrow\rangle, |\mathrm{f}_{xyz},\uparrow\rangle, |\mathrm{f}_{xyz},\downarrow\rangle)^{\mathrm{T}}$. Here $\delta_1 = (x+y)/\sqrt{2}$ and $\delta_2 = (-x+y)/\sqrt{2}$ form a vortex with winding number 1.[12] Then Eq. (1) can be written in a matrix form:

$$\mathcal{H}(k_z) = \begin{pmatrix} \mathcal{H}_1(k_z) & 0 \\ 0 & \mathcal{H}_2(k_z) \end{pmatrix}, \tag{2}$$

where

$$\mathcal{H}_1(k_z) = \begin{pmatrix} \delta_1 & 0 & k_z - \mathrm{i}\delta_2 & -\mathrm{i}\partial_x - \partial_y \\ 0 & \delta_1 & -\mathrm{i}\partial_x + \partial_y & -k_z - \mathrm{i}\delta_2 \\ k_z + \mathrm{i}\delta_2 & -\mathrm{i}\partial_x - \partial_y & -\delta_1 & 0 \\ -\mathrm{i}\partial_x + \partial_y & -k_z + \mathrm{i}\delta_2 & 0 & -\delta_1 \end{pmatrix}, \tag{3}$$

$$\mathcal{H}_2(k_z) = \begin{pmatrix} \delta_1 & 0 & k_z + \mathrm{i}\delta_2 & -\mathrm{i}\partial_x - \partial_y \\ 0 & \delta_1 & -\mathrm{i}\partial_x + \partial_y & -k_z + \mathrm{i}\delta_2 \\ k_z - \mathrm{i}\delta_2 & -\mathrm{i}\partial_x - \partial_y & -\delta_1 & 0 \\ -\mathrm{i}\partial_x + \partial_y & -k_z - \mathrm{i}\delta_2 & 0 & -\delta_1 \end{pmatrix}. \tag{4}$$

We apply a similarity transformation $R = \exp(\frac{\mathrm{i}\pi}{4}\rho_z\tau_y\sigma_0)$ on the Hamiltonian (1), and choose $k_z = 0$. After an elementary transformation, the matrix form becomes a block anti-diagonal matrix form:

$$H(k_z = 0) = \begin{pmatrix} 0 & 0 & 0 & h_1 \\ 0 & 0 & h_2 & 0 \\ 0 & h_2^\dagger & 0 & 0 \\ h_1^\dagger & 0 & 0 & 0 \end{pmatrix}, \tag{5}$$

with

$$h_1 = \begin{pmatrix} \mathrm{i}\partial_x + \partial_y & \delta_1 + \mathrm{i}\delta_2 \\ \delta_1 - \mathrm{i}\delta_2 & -\mathrm{i}\partial_x + \partial_y \end{pmatrix},$$

$$h_2 = \begin{pmatrix} \mathrm{i}\partial_x - \partial_y & -\delta_1 + \mathrm{i}\delta_2 \\ -\delta_1 - \mathrm{i}\delta_2 & -\mathrm{i}\partial_x - \partial_y \end{pmatrix},$$

$$h_2^\dagger = \begin{pmatrix} \mathrm{i}\partial_x + \partial_y & -\delta_1 + \mathrm{i}\delta_2 \\ -\delta_1 - \mathrm{i}\delta_2 & -\mathrm{i}\partial_x + \partial_y \end{pmatrix},$$

$$h_1^\dagger = \begin{pmatrix} \mathrm{i}\partial_x - \partial_y & \delta_1 + \mathrm{i}\delta_2 \\ \delta_1 - \mathrm{i}\delta_2 & -\mathrm{i}\partial_x - \partial_y \end{pmatrix}.$$

Here we should remind that $(\partial_x)^\dagger = -\partial_x$, $(\partial_y)^\dagger = -\partial_y$, $\delta_1 = (x+y)/\sqrt{2}$, and $\delta_2 = (-x+y)/\sqrt{2}$.

The Hamiltonian $H(k_z)$ has Kramers degenerate zero modes propagating along the hinge when $k_z = 0$.[12] We can solve the eigenequation $H(k_z = 0)(\phi_1, \phi_2, \phi_3, \phi_4, \phi_5, \phi_6, \phi_7, \phi_8)^{\mathrm{T}} = 0$ and decompose it into a series of equations:

$$\begin{aligned} &(\mathrm{i}\partial_x - \partial_y)\phi_1 + \frac{1-\mathrm{i}}{\sqrt{2}}(x+\mathrm{i}y)\phi_2 = 0, \\ &\frac{1+\mathrm{i}}{\sqrt{2}}(x-\mathrm{i}y)\phi_1 - (\mathrm{i}\partial_x + \partial_y)\phi_2 = 0. \end{aligned} \tag{6}$$

Then we can get the separate equation for ϕ_1, i.e.,

$$(x-\mathrm{i}y)\phi_1 - (\partial_x - \mathrm{i}\partial_y)\left[\frac{1}{x+\mathrm{i}y}(\partial_x + \mathrm{i}\partial_y)\phi_1\right] = 0, \tag{7}$$

and arrive at the equation

$$\begin{aligned} &x\partial_x^2 X(x)Y(y) + x\partial_y^2 X(x)Y(y) - 2\partial_x X(x)Y(y) \\ &-x(x^2+y^2)X(x)Y(y) = 0 \end{aligned} \tag{8}$$

by setting $\phi_1 = X(x)Y(y)$.

After some standard derivations of solving the equation, we can get the solutions as

$$X(x) = Y(x) = \frac{(c_1 - \mathrm{i}c_2)}{2}\mathrm{e}^{-\frac{x^2}{2}} + \frac{(c_1 + \mathrm{i}c_2)}{2}\mathrm{e}^{\frac{x^2}{2}}, \tag{9}$$

with constants c_1 and c_2. We have to discard the $\exp(x^2/2)$ part for the sake of the physical reason of the wave function. Then the $\phi_1(x,y) = X(x)Y(y) = c\,\mathrm{e}^{-\frac{x^2+y^2}{2}}$ with complex constant c, and similarly $\phi_2 = c\frac{(\mathrm{i}-1)}{\sqrt{2}}\mathrm{e}^{-\frac{x^2+y^2}{2}}$. Furthermore, the eigenmodes of $H(k_z = 0)$ can be derived by computing the remaining equations. These will consist of two counter-propagating Kramers paired eigenmodes:

$$\psi_1 = c\,\mathrm{e}^{-\frac{x^2+y^2}{2}}\left(1, \frac{(\mathrm{i}-1)}{\sqrt{2}}, 0, 0, 0, 0, 0, 0\right)^{\mathrm{T}}, \tag{10}$$

$$\psi_2 = c\,\mathrm{e}^{-\frac{x^2+y^2}{2}}\left(0, 0, \frac{(\mathrm{i}-1)}{\sqrt{2}}, 1, 0, 0, 0, 0\right)^{\mathrm{T}}, \tag{11}$$

with c being the appropriate normalization factor. The dispersion about k_z can be inferred from the matrix elements

$$\begin{pmatrix} \langle\psi_1|H(k_z)|\psi_1\rangle & \langle\psi_1|H(k_z)|\psi_2\rangle \\ \langle\psi_2|H(k_z)|\psi_1\rangle & \langle\psi_2|H(k_z)|\psi_2\rangle \end{pmatrix} = \begin{pmatrix} -k_z & 0 \\ 0 & k_z \end{pmatrix}. \tag{12}$$

The eigenmode $|\psi_+\rangle = |\psi_2\rangle$ when eigenvalue $\varepsilon = k_z$ and $|\psi_-\rangle = |\psi_1\rangle$ when $\varepsilon = -k_z$.

In the presence of magnetic impurities within the helical hinge, the interaction between impurity $\boldsymbol{S}_i$ and itinerant carriers $\boldsymbol{\sigma}$ can be expressed as

$$H_i^{\mathrm{int}} = J(\tau_0 + \tau_x) \otimes (\boldsymbol{\sigma}\cdot\boldsymbol{S}_i)\delta(z - z_i), \tag{13}$$

where constant J is coupling strength, τ_0 and τ_x are matrices acting on the same orbitals as in Eq. (1). Here, $\tau_0 + \tau_x$ means that both the d and f orbitals contribute to the interaction; $\boldsymbol{\sigma} = (\sigma_x, \sigma_y, \sigma_z)$ is for the spin vector of carriers, and $\boldsymbol{S}_i = (S_{ix}, S_{iy}, S_{iz})$ for the spin vector of impurities; $\delta(z - z_i)$ is Dirac δ-function which means that such interaction is a short-range contact exchange interaction.[40,41]

3. RKKY interaction in helical hinges

First, we consider the RKKY interaction mediating by itinerant carriers between two impurities with localized spin in the hinge of helical HOTIs. The RKKY interaction between impurity 1 and 2 can be calculated by

$$H_{1,2}^{\mathrm{RKKY}} = -\frac{1}{\pi}\mathrm{Im}\int_{-\infty}^{\varepsilon_{\mathrm{F}}} \mathrm{Tr}[H_1^{\mathrm{int}} G_1(z,\varepsilon) H_2^{\mathrm{int}} G_2(-z,\varepsilon)]\,\mathrm{d}\varepsilon, \tag{14}$$

where ε_{F} is Fermi energy and $G(z,\varepsilon)$ is the real space Green's function of the itinerant carriers.

Note that the momentum k_x and k_y are not good quantum numbers, and we cannot write the momentum space Green's function directly. However, we can write Green's function in the eigenspace of $H(k_z)$ instead. For simplicity, we rewrite the eigenstates Eq. (10) in the subspace $\boldsymbol{\tau}\otimes\boldsymbol{\sigma}$, and the corresponding bases are $(\tau_+\uparrow, \tau_+\downarrow, \tau_-\uparrow, \tau_-\downarrow)^{\mathrm{T}}$, where $\tau_{+(-)}$ stands for d (f) orbitals and $\uparrow$ ($\downarrow$) stands for spin up (down). The rewritten eigenstates are

$$|\psi_+\rangle = N\mathrm{e}^{-\frac{x^2+y^2}{2}}|\tau_-\rangle\left(\frac{(\mathrm{i}-1)}{\sqrt{2}}|\uparrow\rangle + |\downarrow\rangle\right), \tag{15}$$

$$|\psi_-\rangle = N\mathrm{e}^{-\frac{x^2+y^2}{2}}|\tau_+\rangle\left(|\uparrow\rangle + \frac{(\mathrm{i}-1)}{\sqrt{2}}|\downarrow\rangle\right). \tag{16}$$

In the eigenspace of $H(k_z)$, Green's function is

$$G(k_z,\varepsilon) = \frac{\psi_+(x,y)\psi_+^\dagger(x',y')}{(\varepsilon + \mathrm{i}0^+) - k_z} + \frac{\psi_-(x,y)\psi_-^\dagger(x',y')}{(\varepsilon + \mathrm{i}0^+) + k_z}. \tag{17}$$

The corresponding matrix form is

$$\begin{aligned} G(k_z,\varepsilon) &= \begin{pmatrix} G_{\tau_+\uparrow\tau_+\uparrow} & G_{\tau_+\uparrow\tau_+\downarrow} & G_{\tau_+\uparrow\tau_-\uparrow} & G_{\tau_+\uparrow\tau_-\downarrow} \\ G_{\tau_+\downarrow\tau_+\uparrow} & G_{\tau_+\downarrow\tau_+\downarrow} & G_{\tau_+\downarrow\tau_-\uparrow} & G_{\tau_+\downarrow\tau_-\downarrow} \\ G_{\tau_-\uparrow\tau_+\uparrow} & G_{\tau_-\uparrow\tau_+\downarrow} & G_{\tau_-\uparrow\tau_-\uparrow} & G_{\tau_-\uparrow\tau_-\downarrow} \\ G_{\tau_-\downarrow\tau_+\uparrow} & G_{\tau_-\downarrow\tau_+\downarrow} & G_{\tau_-\downarrow\tau_-\uparrow} & G_{\tau_-\downarrow\tau_-\downarrow} \end{pmatrix} \\ &= \frac{1}{2\pi}\mathrm{e}^{-\frac{x^2+y^2+x'^2+y'^2}{2}}\begin{pmatrix} G_{11} & 0 \\ 0 & G_{22} \end{pmatrix}, \end{aligned} \tag{18}$$

with

$$G_{11} = \begin{pmatrix} \frac{1}{(\varepsilon+\mathrm{i}0^+)+k_z} & \frac{(-\mathrm{i}-1)}{\sqrt{2}}\frac{1}{(\varepsilon+\mathrm{i}0^+)+k_z} \\ \frac{(\mathrm{i}-1)}{\sqrt{2}}\frac{1}{(\varepsilon+\mathrm{i}0^+)+k_z} & \frac{1}{(\varepsilon+\mathrm{i}0^+)+k_z} \end{pmatrix}, \tag{19}$$

$$G_{22} = \begin{pmatrix} \frac{1}{(\varepsilon+\mathrm{i}0^+)-k_z} & \frac{(\mathrm{i}-1)}{\sqrt{2}}\frac{1}{(\varepsilon+\mathrm{i}0^+)-k_z} \\ \frac{(-\mathrm{i}-1)}{\sqrt{2}}\frac{1}{(\varepsilon+\mathrm{i}0^+)-k_z} & \frac{1}{(\varepsilon+\mathrm{i}0^+)-k_z} \end{pmatrix}. \tag{20}$$

One intriguing observation is that the propagator G_{11} possesses a momentum of $-k_z$ and a $SU(2)$ structure of $(-\sigma_x + \sigma_y)$, while the propagator G_{22} contains k_z and $(-\sigma_x - \sigma_y)$,

potentially due to the spin–momentum locking of the helical hinge states.

After the Fourier transformation, we can get the real-space Green function

$$G(z,\varepsilon)=\frac{\mathrm{i}}{4\pi}\mathrm{e}^{-\frac{(x^2+y^2+x'^2+y'^2)}{2}}\begin{pmatrix} g_{11} & 0\\ 0 & g_{22}\end{pmatrix}, \tag{21}$$

with

$$g_{11}=\mathrm{e}^{-\mathrm{i}\varepsilon z}\begin{pmatrix} (\mathrm{sgn}[z]-1) & (\mathrm{sgn}[z]-1)\frac{(-\mathrm{i}-1)}{\sqrt{2}}\\ (\mathrm{sgn}[z]-1)\frac{(\mathrm{i}-1)}{\sqrt{2}} & (\mathrm{sgn}[z]-1)\end{pmatrix}, \tag{22}$$

$$g_{22}=\mathrm{e}^{\mathrm{i}\varepsilon z}\begin{pmatrix} (\mathrm{sgn}[z]+1) & (\mathrm{sgn}[z]+1)\frac{(\mathrm{i}-1)}{\sqrt{2}}\\ (\mathrm{sgn}[z]+1)\frac{(-\mathrm{i}-1)}{\sqrt{2}} & (\mathrm{sgn}[z]+1)\end{pmatrix}, \tag{23}$$

where $\mathrm{sgn}[z]$ is the sign function. We can see that $g_{11(22)}=0$ when $z>0$ ($z<0$), indicating Green's function depends on the f (d) orbitals. This peculiar dependence on the sign of z implies that the helicity of Green's functions, i.e., the propagator, is direction-dependent.

Then we can reach the RKKY interaction of HOTI in the helical hinge:

$$\begin{aligned}H_{1,2}^{\mathrm{RKKY}}=&F_1(z,\varepsilon_{\mathrm{F}})(\boldsymbol{S}_1\cdot\boldsymbol{S}_2+S_{1x}S_{2x}-S_{1y}S_{2y})\\&+F_2(z,\varepsilon_{\mathrm{F}})(\boldsymbol{S}_1\times\boldsymbol{S}_2)_y,\end{aligned} \tag{24}$$

with

$$F_1(z,\varepsilon_{\mathrm{F}})=\frac{J^2}{4\pi^3|z|}[\cos(2z\varepsilon_{\mathrm{F}})-1]\,\mathrm{e}^{-(x^2+y^2+x'^2+y'^2)}, \tag{25}$$

$$F_2(z,\varepsilon_{\mathrm{F}})=-\frac{\sqrt{2}J^2}{4\pi^3|z|}\sin(2z\varepsilon_{\mathrm{F}})\,\mathrm{e}^{-(x^2+y^2+x'^2+y'^2)}, \tag{26}$$

by combining Eqs. (13), (14) and (21) and introducing a cutoff function $\exp(-\varepsilon^2/\Lambda^2)$ with $\Lambda\to 0$. We can turn the analytical expressions to the International System of Units for facilitating the experimentalists:

$$\begin{aligned}F_1(z,\varepsilon_{\mathrm{F}})=&\frac{am_0\hbar^{-2}J^2}{4\pi^3|z|}[\cos(2am_0\hbar^{-2}z\varepsilon_{\mathrm{F}})-1]\\&\times\mathrm{e}^{-a^{-2}(x^2+y^2+x'^2+y'^2)},\end{aligned} \tag{27}$$

$$\begin{aligned}F_2(z,\varepsilon_{\mathrm{F}})=&-\frac{\sqrt{2}am_0\hbar^{-2}J^2}{4\pi^3|z|}\sin(2am_0\hbar^{-2}z\varepsilon_{\mathrm{F}})\\&\times\mathrm{e}^{-a^{-2}(x^2+y^2+x'^2+y'^2)},\end{aligned} \tag{28}$$

where $\hbar$ is the reduced Planck constant, and a is half crystal constant of SnTe about 0.316 nm.[12,42] We take spin–spin coupling constant $J=10$ meV·nm. It should be noted that there exist two non-equivalent branches ($z>0$ and $z<0$), and the only factor that sets them apart for a given inter-impurity distance is the sign of the DM term, indicating the helicity type. Here Fermi energy $\varepsilon_{\mathrm{F}}>0$ (<0) corresponds to n-type (p-type) doping. The different types of doping cause a sign reversal of the DM interaction $(\boldsymbol{S}_1\times\boldsymbol{S}_2)_y$. The long-range asymptotic behavior of the RKKY interaction is

$$\begin{aligned}H_{1,2}^{\mathrm{RKKY}}(z\to\infty)\simeq&\frac{1}{z}[\boldsymbol{S}_1\cdot\boldsymbol{S}_2+S_{1x}S_{2x}-S_{1y}S_{2y}\\&-(\boldsymbol{S}_1\times\boldsymbol{S}_2)_y].\end{aligned} \tag{29}$$

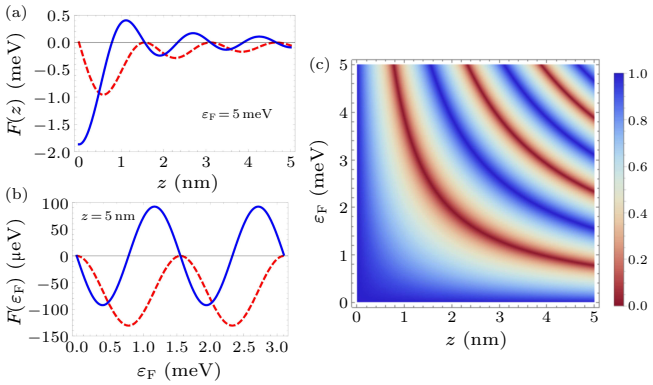


Fig. 2. Helical HOTIs' range functions depending on (a) the impurity spacing z, (b) the Fermi energy ε_{F}, and (c) the proportion of DM interaction. (a) The range functions oscillating decay with impurity spacing z at $\varepsilon_{\mathrm{F}}=5$ meV. (b) The range functions depending on the Fermi energy ε_{F} oscillate with the same period as simple sine functions corresponding to impurity spacing $z=5$ nm. The red solid line stands for the collinear terms F_1 and the blue dashed line stands for the non-collinear term (DM interaction) F_2. (c) The proportion of DM interaction in the total RKKY interaction $|F_2|/(|F_1|+|F_2|)$ depending on the impurity spacing z and the Fermi energy ε_{F}. We take coupling strength $J=10$ meV·nm.

The range functions depend on the impurity spacing z, the Fermi energy ε_{F} and the distribution of carriers in xy plane. In Fig. 2(a), we can see that the range functions $F_1(z,\varepsilon_{\mathrm{F}}),F_2(z,\varepsilon_{\mathrm{F}})$ depend on the impurity spacing z, showing the same damped oscillatory behavior. The hinge RKKY interaction decays as z^{-1}, which is in line with the previous results of the RKKY interaction in helical edges of topological superconductors.[43] The 1D topological higher-order boundary could slow down the decay of the RKKY interaction from $1/z^2$ of the 2D common topological surface[34,37,39] to $1/z$, and hence drastically enhances its magnitude. This stronger RKKY interaction in 1D nontrivial helical hinge is more promising for potential applications in topological spintronics. In helical HOTIs, the Heisenberg- and Ising-type interactions are always ferromagnetic while DM-type interaction shows anisotropic gyromagnetism. With increasing Fermi energy ε_{F}, the range functions of helical HOTIs show the simple sine function oscillating behavior with the same period, as shown in Fig. 2(b). If we finely tune the parameters z and ε_{F}, we can get different spin interactions within different regimes of the parameters. For example, the RKKY interaction reduces to a pure DM interaction when the inter-impurity distance and the Fermi energy are rather small, and the RKKY interaction reduces to a anisotropic Heisenberg interaction when the inter-impurity distance and the Fermi energy reach the critical values $z\varepsilon_{\mathrm{F}}=(n+1/2)\pi$. Figure 2(c) shows the proportion of DM interaction in the total RKKY interaction. We can see that the proportion oscillate

with increasing impurity spacing z and the Fermi energy $\varepsilon_{\rm F}$, and we can finely tune the hinge RKKY interaction between the collinear anisotropic Heisenberg interaction and the non-collinear DM interaction.

The distribution of the range function F_1 in the xy plane depending on both inter-impurity distance z and the Fermi energy $\varepsilon_{\rm F}$ is shown in Fig. 3(a). The range functions are isotropic in the xy plane and decrease exponentially, which is a natural consequence resulting from the trivial bulk states. The range function F_2 shows exactly the same behavior as F_1. When the impurities locate off the hinge, for instance, $x = 0.1$ nm, $y = 0.1$ nm, the RKKY interaction show almost the same behavior as in the hinge, except for a decrease in magnitude, as shown in Fig. 3(b). The robust nature of the hinge RKKY interaction guarantees the durability of the spintronic devices that may be realized in the helical hinge of HOTIs. We also show the distribution of range functions F_1 and F_2 depending on coordinates y and z in Figs. 3(c) and 3(d), which clearly indicate an oscillatory decay pattern along the z axis and an exponential decay along the y axis.

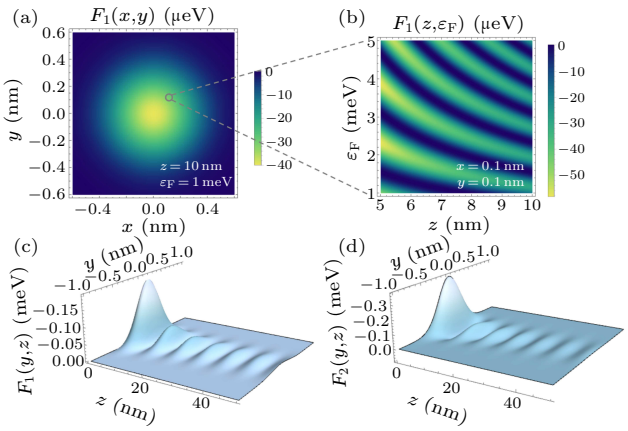


Fig. 3. (a) The isotropic and exponential decayed distribution of range function F_1 in the xy plane corresponding to $z = 10$ nm and $\varepsilon_{\rm F} = 1$ meV. (b) The range function F_1 of the hinge at $x = 0.1$, $y = 0.1$ nm depending on the impurity spacing z and the Fermi energy $\varepsilon_{\rm F}$. [(c), (d)] The distributions of the range function F_1 and F_2 in yz plane at $x = 0$, $\varepsilon_{\rm F} = 1$ meV.

4. RKKY interaction in the Dirac-type bulk states

For bulk doping, density functional theory calculations[44–46] and quantum Monte Carlo calculation[47] find a complicated anisotropic spin texture in magnetically doped TIs. Therefore, the 3D Dirac-type bulk states attribute to the RKKY interaction in the doped regimes, and may also induce the complicated RKKY interaction due to the profound relation between the bulk states and the hinge states. This relation is reflected by the fact that the Hamiltonian of hinge states is derived from the Dirac-type bulk Hamiltonian of HOTIs. Here we start from the 3D Dirac-type bulk Hamiltonian[12]

$$H_b(\boldsymbol{k}) = k_x\tau_x\sigma_x + k_y\tau_x\sigma_y + k_z\tau_x\sigma_z, \tag{30}$$

where the Pauli matrixes τ and σ are defined as above. We examine the bulk RKKY interaction in the helical HOTIs. Green's function in momentum space can be calculated directly by

$$G(\boldsymbol{k},\varepsilon) = \frac{\varepsilon\tau_0\sigma_0 + \tau_x\boldsymbol{k}\cdot\boldsymbol{\sigma}}{\varepsilon^2 - k^2}. \tag{31}$$

By applying Fourier transform on $G(\boldsymbol{k},\varepsilon)$, we can arrive at Green's function in real space

$$G(\boldsymbol{R},\varepsilon) = \frac{1}{(2\pi)^3}\int G(\boldsymbol{k},\varepsilon)\mathrm{e}^{\mathrm{i}\boldsymbol{k}\cdot\boldsymbol{R}}\mathrm{d}^3\boldsymbol{k}. \tag{32}$$

We can replace $\boldsymbol{k}$ with $\boldsymbol{k}_\parallel + \boldsymbol{k}_\perp$, where $\boldsymbol{k}_\parallel$ is the part parallel to $\boldsymbol{R}$ and $\boldsymbol{k}_\perp$ the perpendicular part. For $\boldsymbol{k}_\perp\cdot\boldsymbol{R} = 0$, we have

$$\begin{aligned} G(\boldsymbol{R},\varepsilon) =& \frac{1}{(2\pi)^3}\int\frac{\varepsilon\tau_0\sigma_0 + \tau_x(\boldsymbol{k}_\parallel + \boldsymbol{k}_\perp)\cdot\boldsymbol{\sigma}}{\varepsilon^2 - k^2}\mathrm{e}^{\mathrm{i}\boldsymbol{k}_\parallel\cdot\boldsymbol{R}}\mathrm{d}^3\boldsymbol{k} \\ =& \frac{-\varepsilon\mathrm{e}^{\mathrm{i}R\varepsilon}}{4\pi R}\tau_0\sigma_0 + \left(\frac{\mathrm{e}^{\mathrm{i}R\varepsilon}}{4\pi\mathrm{i}R^2} - \frac{\varepsilon\mathrm{e}^{\mathrm{i}R\varepsilon}}{4\pi R}\right)\tau_x\hat{\boldsymbol{R}}\cdot\boldsymbol{\sigma}. \end{aligned} \tag{33}$$

Similarly,

$$G(-\boldsymbol{R},\varepsilon) = \frac{-\varepsilon\mathrm{e}^{\mathrm{i}R\varepsilon}}{4\pi R}\tau_0\sigma_0 - \left(\frac{\mathrm{e}^{\mathrm{i}R\varepsilon}}{4\pi\mathrm{i}R^2} - \frac{\varepsilon\mathrm{e}^{\mathrm{i}R\varepsilon}}{4\pi R}\right)\tau_x\hat{\boldsymbol{R}}\cdot\boldsymbol{\sigma}. \tag{34}$$

The interaction Hamiltonian is

$$H_i^{\rm int} = J(\tau_0 + \tau_x)\otimes(\boldsymbol{\sigma}\cdot\boldsymbol{S}_i)\delta(\boldsymbol{R} - \boldsymbol{R}_i). \tag{35}$$

After a standard derivation of the RKKY interaction by the integral

$$\begin{aligned} &H_{\rm bulk1,2}^{\rm RKKY} \\ &= -\frac{1}{\pi}\mathrm{Im}\int_{-\infty}^{\varepsilon_{\rm F}}\mathrm{Tr}[H_1^{\rm int}G_1(\boldsymbol{R},\varepsilon)H_2^{\rm int}G_2(-\boldsymbol{R},\varepsilon)]\,\mathrm{d}\varepsilon, \end{aligned} \tag{36}$$

we finally get the bulk RKKY interaction depending on the orientation of two impurities

$$\begin{aligned} H_{\rm bulk1,2}^{\rm RKKY} =& f_1(R,\varepsilon_{\rm F})\boldsymbol{S}_1\cdot\boldsymbol{S}_2 + f_2(R,\varepsilon_{\rm F})\boldsymbol{S}_1\cdot\boldsymbol{M}\cdot\boldsymbol{S}_2 \\ &+ f_3(R,\varepsilon_{\rm F})\boldsymbol{n}\cdot(\boldsymbol{S}_1\times\boldsymbol{S}_2), \end{aligned} \tag{37}$$

with

$$\begin{aligned} f_1(R,\varepsilon_{\rm F}) =& \frac{J^2}{8\pi^3R^5}[-\cos(2R\varepsilon_{\rm F}) - 2R\varepsilon_{\rm F}\sin(2R\varepsilon_{\rm F}) \\ &+ 2R^2\varepsilon_{\rm F}^2\cos(2R\varepsilon_{\rm F})], \end{aligned} \tag{38}$$

$$\begin{aligned} f_2(R,\varepsilon_{\rm F}) =& \frac{J^2}{16\pi^3R^5}[-5\cos(2R\varepsilon_{\rm F}) - 6R\varepsilon_{\rm F}\sin(2R\varepsilon_{\rm F}) \\ &+ 2R^2\varepsilon_{\rm F}^2\cos(2R\varepsilon_{\rm F})], \end{aligned} \tag{39}$$

$$\begin{aligned} f_3(R,\varepsilon_{\rm F}) =& \frac{J^2}{2\pi^3R^5}[-\sin(2R\varepsilon_{\rm F}) + 2R\varepsilon_{\rm F}\cos(2R\varepsilon_{\rm F}) \\ &+ R^2\varepsilon_{\rm F}^2\sin(2R\varepsilon_{\rm F})]. \end{aligned} \tag{40}$$

The corresponding International System of Units expressions are omitted here for brevity. The second-order tensor of rotation reads

$$\boldsymbol{M}=\begin{pmatrix} 1+\cos(2\theta)-2\sin^2\theta\cos(2\varphi) & -2\sin^2\theta\sin(2\varphi) & -2\sin(2\theta)\cos\varphi \\ -2\sin^2\theta\sin(2\varphi) & 1+\cos(2\theta)+2\sin^2\theta\cos(2\varphi) & -2\sin(2\theta)\sin\varphi \\ -2\sin(2\theta)\cos\varphi & -2\sin(2\theta)\sin\varphi & \sin^2\theta\sin(2\varphi) \end{pmatrix}, \tag{41}$$

and the orientation vector is $\boldsymbol{n}=(\cos\varphi\sin\theta,\sin\varphi\sin\theta,\cos\theta)$. Here the angle θ is defined between $\boldsymbol{R}$ and z axis, and the angle φ is defined between the projection of $\boldsymbol{R}$ on xy plane and the x axis. The bulk RKKY interaction has complicated formalism consisting of a Heisenberg term, a twisted Ising term, and a DM term along the orientation vector, similar to the RKKY interaction in TI, topological semimetal and systems with spin–orbit coupling.[35,39,48–51]

The long-range asymptotic behavior of the RKKY interaction is

$$H^{\mathrm{RKKY}}_{\mathrm{bulk}1,2}(R\to\infty)\simeq\frac{1}{R^3}[\boldsymbol{S}_1\cdot\boldsymbol{S}_2+\boldsymbol{S}_1\cdot\boldsymbol{M}\cdot\boldsymbol{S}_2 +\boldsymbol{n}\cdot(\boldsymbol{S}_1\times\boldsymbol{S}_2)]. \tag{42}$$

Notice that the range function monotonically decreases as $1/R^3$ in this case, as the same as the conventional RKKY interaction.

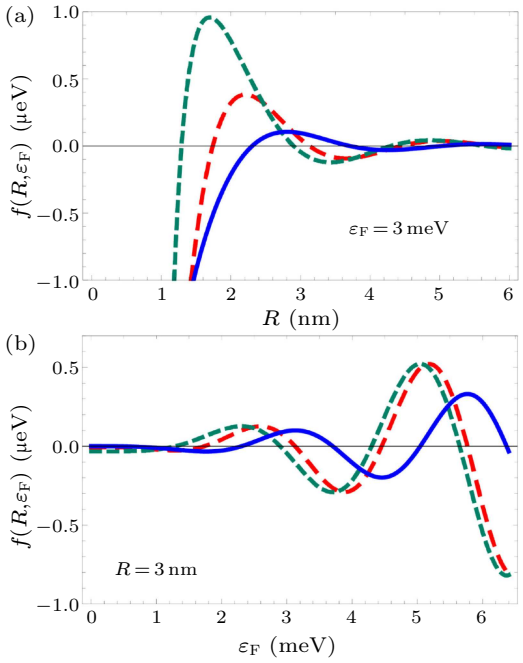


Fig. 4. (a) The bulk's range functions $f_1(R,\varepsilon_F)$, $f_2(R,\varepsilon_F)$, $f_3(R,\varepsilon_F)$ depending on impurity spacing R at Fermi energy $\varepsilon_F=3$ meV denoted by red (long-dashed), green (short-dashed), blue (solid) lines, respectively. These range functions oscillate with the same period and decay with R^{-3} asymptotically. (b) The bulk's range functions depending on Fermi energy ε_F at impurity spacing $R=3$ nm.

The range functions of bulk RKKY interaction are shown in Fig. 4 and depend on impurity spacing R and Fermi energy ε_F. We can see that the bulk RKKY interaction decay much faster (R^{-3}) than the hinge RKKY interaction (R^{-1}) in Fig. 4(a). The range functions show the conventional oscillating decay behavior as in normal metals and semiconductors. The primary distinction between the bulk and hinge RKKY interactions is the different dependencies on the Fermi energy ε_F. The range functions of bulk RKKY interaction exhibit greater oscillation with increasing Fermi energy. All these range functions oscillate with the same period.

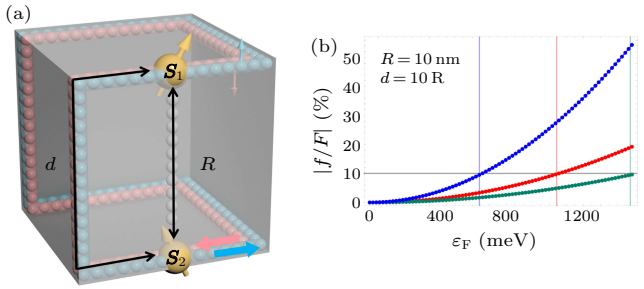


Fig. 5. (a) Schematic diagram of RKKY interaction mediated by both hinge and bulk carriers between impurities in complex configuration. The distance corresponding to bulk carriers is specified as R, while for hinge carriers it is indicated as d. We take the hinge spacing $R=1$ nm and the bulk spacing $d=10\,R$. (b) Percentage of bulk to hinge correction depending on the Fermi energy ε_F at $R=10$ nm, $d=10\,R$. The red, green and blue lines stand for the Heisenberg, (twisted) Ising and DM terms, respectively. Here the values of range functions are represented by the minimum in every period.

The RKKY interaction can be mediated by both the helical itinerant carriers and the Dirac bulk carriers in the doped regime, as shown in Fig. 5(a). At appropriate parameter selection, the contributions of hinge and bulk to RKKY interaction are comparable. We show the correction of the bulk RKKY interaction to the hinge RKKY interaction when the Fermi energy increases, as shown in Fig. 5(b). The proportion f/F change with ε_F^2. The contribution of the bulk RKKY interaction is more than 10% of the hinge RKKY interaction when the Fermi energy is about 1100 meV for the Heisenberg term, 1510 meV for the (twisted) Ising term and 620 meV for the DM term. By adjusting the Fermi energy, we can utilize this phenomena to effectively transform the RKKY interaction into a dominant DM term within the spin interaction formalism.

5. Conclusions

In conclusion, our theoretical exploration of the RKKY interaction within helical HOTIs unveils distinct interaction mechanisms mediated by hinge and Dirac-type bulk carriers. Specifically, we find that the hinge-mediated RKKY interaction encompasses a comprehensive suite of terms: the Heisenberg, x-Ising, y-Ising, and DM terms, with the latter oriented along the y direction. Notably, these interactions exhibit a decay proportional to z^{-1} with increasing impurity spacing, and oscillate in strength according to sine functions as a function of the Fermi energy, ε_F. This behavior underscores a consistent ferromagnetic coupling in both Heisenberg-type and Ising-type interactions, while DM-type interactions demonstrate alternating behaviors. Moreover, the isotropic decay of these

interactions in the *xy* plane further delineates the nuanced role of hinge carriers. Conversely, interactions mediated by bulk carriers are characterized by Heisenberg, twisted Ising, and DM terms, showcasing a R^{-3} decay and conventional oscillatory decay with increased impurity spacing. The interplay between hinge and bulk interactions presents a fertile ground for developing advanced quantum devices, leveraging the unique properties of helical HOTIs. Our findings not only deepen the understanding of RKKY interactions in these novel materials but also open avenues for designs of next-generation spintronics devices, capitalizing on the intricate interplay of hinge and bulk carrier dynamics.

Acknowledgment

This work was supported by the research foundation of Institute for Advanced Sciences of CQUPT (Grant No. E011A2022328).

References

[1] Kim M, Jacob Z and Rho J 2020 *Light Sci. Appl.* **9** 130
[2] Xie B, Wang H X, Zhang X, Zhan P, Jiang J H, Lu M and Chen Y 2021 *Nat. Rev. Phys.* **3** 520
[3] Benalcazar W A, Bernevig B A and Hughes T L 2017 *Science* **357** 61
[4] Liu F and Wakabayashi K 2017 *Phys. Rev. Lett.* **118** 076803
[5] Lin Z K, Wu S Q, Wang H X and Jiang J H 2020 *Chin. Phys. Lett.* **37** 074302
[6] Chen H, Liu Z R, Chen R and Zhou B 2024 *Chin. Phys. B* **33** 01720
[7] Ni X, Li M, Weiner M, Alù A and Khanikaev A B 2020 *Nat. Commun.* **11** 2108
[8] Liu S, Ma S, Zhang Q, Zhang L, Yang C, You O, Gao W, Xiang Y, Cui T J and Zhang S 2020 *Light Sci. Appl.* **9** 145
[9] Hackenbroich A, Hudomal A, Schuch N, Bernevig B A and Regnault N 2021 *Phys. Rev. B* **103** L161110
[10] Wang J H, Yang Y B, Dai N and Xu Y 2021 *Phys. Rev. Lett.* **126** 206404
[11] Fu B, Hu Z A and Shen S Q 2021 *Phys. Rev. Res.* **3** 033177
[12] Schindler F, Cook A M, Vergniory M G, Wang Z, Parkin S S, Bernevig B A and Neupert T 2018 *Sci. Adv.* **4** eaat0346
[13] Hsieh T H, Lin H, Liu J, Duan W, Bansil A and Fu L 2012 *Nat. Commun.* **3** 982
[14] Tanaka Y, Ren Z, Sato T, Nakayama K, Souma S, Takahashi T, Segawa K and Ando Y 2012 *Nat. Phys.* **8** 800
[15] Benalcazar W A, Bernevig B A and Hughes T L 2017 *Phys. Rev. B* **96** 245115
[16] Sessi P, Sante D D, Szczerbakow A, Glott F, Wilfert S, Schmidt H, Bathon T, Dziawa P, Greiter M, Neupert T, Sangiovanni G, Story T, Thomale R and Bode M 2016 *Science* **354** 1269
[17] Bernevig B A and Zhang S C 2006 *Phys. Rev. Lett.* **96** 106802
[18] Fang C and Fu L 2019 *Sci. Adv.* **5** eaat2374
[19] Kohda M, Okayasu T and Nitta J 2019 *Sci. Rep.* **9** 1909
[20] Yang Z Q, Shao Z K, Chen H Z, Mao X R and Ma R M 2020 *Phys. Rev. Lett.* **125** 013903
[21] Aggarwal L, Zhu P, Hughes T L and Madhavan V 2021 *Nat. Commun.* **12** 4420
[22] Schindler F, Wang Z, Vergniory M G, Cook A M, Murani A, Sengupta S, Kasumov A Y, Deblock R, Jeon S, Drozdov I, Bouchiat H, Guéon S, Yazdani A, Bernevig B A and Neupert T 2018 *Nat. Phys.* **14** 918
[23] Hsu C H, Zhou X, Ma Q, Gedik N, Bansil A, Pereira V M, Lin H, Fu L, Xu S Y and Chang T R 2019 *2D Mater.* **6** 031004
[24] Shumiya N, Hossain M S, Yin J X, *et al.* 2022 *Nat. Mater.* **21** 1111
[25] Wang Z, Wieder B J, Li J, Yan B and Bernevig B A 2019 *Phys. Rev. Lett.* **123** 186401
[26] Noguchi R, Kobayashi M, Jiang Z, *et al.* 2021 *Nat. Mater.* **20** 473
[27] Laubscher K, Keizer P and Klinovaja J 2023 *Phys. Rev. B* **107** 045409
[28] Yang Z Z, Li X, Peng Y Y, Zou X Y and Cheng J C 2020 *Phys. Rev. Lett.* **125** 255502
[29] Craig N, Taylor J, Lester E, Marcus C, Hanson M and Gossard A 2004 *Science* **304** 565
[30] Usaj G, Lustemberg P and Balseiro C A 2005 *Phys. Rev. Lett.* **94** 036803
[31] Dugaev V K, Litvinov V I and Barnas J 2006 *Phys. Rev. B* **74** 224438
[32] Brey L, Fertig H A and Das Sarma S 2007 *Phys. Rev. Lett.* **99** 116802
[33] Liu Q, Liu C X, Xu C, Qi X L and Zhang S C 2009 *Phys. Rev. Lett.* **102** 156603
[34] Zhu J J, Yao D X, Zhang S C and Chang K 2011 *Phys. Rev. Lett.* **106** 097201
[35] Chang H R, Zhou J, Wang S X, Shan W Y and Xiao D 2015 *Phys. Rev. B* **92** 241103
[36] Hosseini M V and Askari M 2015 *Phys. Rev. B* **92** 224435
[37] Yarmohammadi M and Cheraghchi H 2020 *Phys. Rev. B* **102** 075411
[38] Cheraghchi H and Yarmohammadi M 2021 *Sci. Rep.* **11** 5273
[39] Yarmohammadi M, Bukov M and Kolodrubetz M H 2023 *Phys. Rev. B* **107** 054439
[40] Hickel T and Nolting W 2004 *Phys. Rev. B* **69** 085110
[41] Nolting W, Reddy G G, Ramakanth A and Meyer D 2001 *Phys. Rev. B* **64** 155109
[42] Schindler F, Tsirkin S S, Neupert T, Bernevig B A and Wieder B J 2022 *Nat. Commun.* **13** 5791
[43] Laubscher K, Miserev D, Kaladzhyan V, Loss D and Klinovaja J 2023 *Phys. Rev. B* **107** 115421
[44] Schmidt T M, Miwa R H and Fazzio A 2011 *Phys. Rev. B* **84** 245418
[45] Henk J, Ernst A, Eremeev S V, Chulkov E V, Maznichenko I V and Mertig I 2012 *Phys. Rev. Lett.* **108** 206801
[46] Zhang J M, Zhu W, Zhang Y, Xiao D and Yao Y 2012 *Phys. Rev. Lett.* **109** 266405
[47] Sun J, Chen L and Lin H Q 2014 *Phys. Rev. B* **89** 115101
[48] Duan H J, Wu Y J, Yang Y Y, Zheng S H, Zhu C Y, Deng M X, Yang M and Wang R Q 2022 *New J. Phys.* **24** 033029
[49] Mohammadi R G and Moghaddam A G 2020 *Phys. Rev. B* **101** 075421
[50] Mross D F and Johannesson H 2009 *Phys. Rev. B* **80** 155302
[51] Duan H J, Wang C, Zheng S H, Wang R Q, Pan D R and Yang M 2018 *Sci. Rep.* **8** 6185